THE INFLUENCE OF LIGHT BEAM CONVERGENCE ON THE STOP-BANDS OF A ONE-DIMENSIONAL PHOTONIC CRYSTAL

Vladimir A. Tolmachev[1], Kevin Berwick[2], and Tatiana S. Perova[3], *

[1]Ioffe Physical Technical Institute, Polytechnicheskaya 26, St.-Petersburg, Russia

[2]School of Electronic and Communications Engineering, Dublin Institute of Technology, Kevin St., Dublin 8, Ireland

[3]Department of Electronic and Electrical Engineering, Trinity College Dublin, Dublin 2, Ireland

Abstract—The influence of beam convergence on the photonic band-gaps, or stop-bands (SBs), of one-dimensional photonic crystals (1D PCs) is investigated. The investigation is based on an analysis of the gap map obtained from reflection spectra, calculated by the transfer matrix method for various angles of light incidence, φ, and polarisations. The calculated data is compared with reflection spectra taken using Fourier Transform Infrared microspectroscopy. It was found that the introduction of the parameter, $\Delta\varphi$ to account for the focused light beam, for angles up to $20°$, has little effect on the first, or lowest SB and the SBs adjacent to it. However, an increase in the order of the SB causes an increase in the influence of this parameter.

1. INTRODUCTION

Recent advances in micro and nano-structuring technologies allow enormous flexibility in choice of material composition, lattice periodicity and symmetry of the periodic arrangements in photonic structures. These techniques allow the fabrication of one-, two- and three-dimensional Photonic Crystals (PCs) operating over a wide spectral range. For example, a PC with typical dimensions of the order

of millimetres can be used for the manipulation of microwave radiation, while a PC with micron scale dimensions can be used to control radiation in the infrared range [1, 2]. Silicon is a particularly attractive optical material due to its transparency in the Near Infrared (NIR) range, spanning the 1.3 and 1.55 μm telecommunication wavelengths, as well as the middle-infrared and long-wave infrared (or far-infrared) ranges up to 100 μm [3]. In addition, the development of in-plane light emitters and other microphotonic elements based on single crystal Si has allowed the practical realisation of all-silicon optoelectronic circuits [4, 5].

In order to tailor the properties of photonic crystals to optimise them for various applications, an understanding of their optical properties is of crucial importance. Photonic crystals exhibit a number of Photonic Band-Gaps (PBGs) or Stop-Bands (SBs), where the propagation of electromagnetic radiation is forbidden [1]. Despite the fact that the lowest stop-band is generally the most robust in terms of its optical properties, the use of higher order stop-bands is suggested in proposals made for photonic devices recently [6, 7].

The optical properties of PCs, fabricated by various techniques, are typically investigated by spectroscopy, using spectrophotometers over a wide spectral range, from the visible to the far-infrared range (see, for example [8, 9]), or systems comprising an Optical Spectrum Analyser (OSA) with optical fibre coupling [7, 10].

When using a spectrophotometer, it is extremely difficult to obtain measurements from a PC element on the chip, parallel to the chip's substrate, since this requires removal of the sample from the chip. Nevertheless, a number of investigations have been performed on photonic elements integrated into a Si chip, using Fourier Transform Infrared (FTIR) spectrophotometers combined with infrared microscopes (see, for example Refs. [11–13]).

In the studies cited above, as well as in experiments where optical fibres are coupled with an OSA, converging optics are required to study micro objects. Since the incident light beam is focussed, disagreement between the experimental and calculated optical characteristics can be expected, since calculations typically assume that unfocused beams are used.

In this study, we investigate how beam convergence influences the position and shape of SBs in the optical spectra of 1D PCs based on 'Si-Air'. We calculate the spectra obtained for different convergence parameters and compare the results obtained with experimental data registered using FTIR microspectrometry.

2. CALCULATION OF REFLECTION SPECTRA OF 1D PC USING A MODEL INCORPORATING A CONVERGING LIGHT BEAM

Let us start by calculating the reflection spectra, R, for an unfocused beam of light at normal incidence, $\varphi = 0°$, and for $\varphi = 15°$ and $30°$. A schematic diagram of the periodic structure of the 1D PC (Si-Air) used in these calculations, is presented in Fig. 1(a). The number of periods, $m = 4$. The refractive index, n_{Si}, for the high index component (H) is taken to be 3.42, the mid-IR value for Si [14]), while the refractive index for air, the low index component (L), is $n_{air} = 1$. Calculations of the reflection (R) and transmission (T) spectra of this structure are performed using the Transfer Matrix Method [15]. The incoming and outgoing media are air, with a refractive index of $n = 1$.
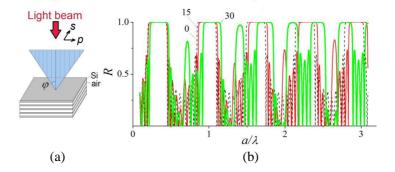

(a)   (b)

Figure 1. (a) Schematic diagram showing light reflection from a 1D PC (layered structure) based on "Si-Air", with number of periods, $m = 4$, for calculation of reflection and transmission spectra; (b) Reflection spectra (in p-polarisation) for a specific angle of light incidence φ, shown by the numbers beside the curves in degrees.

Figure 1(b) shows the p-polarized reflection spectrum, R, at a normal incidence of light, denoted as 0, and at $\varphi = 15°$ and $30°$, denoted as 15 and 30, respectively. The calculation is done for a filling fraction $f_H = d_{Si}/a = 0.23$, corresponding to a quarter wavelength optical thickness for both components. Here, d_{Si} is the geometrical thickness of the Si layers and a is the lattice constant of the periodic structure. The electric vector of the incident light is parallel to the plane of incidence for p-polarized light. Wavelength values, λ, are shown in units of normalized frequency, a/λ, on the X-axis. From Fig. 1(b), for oblique incidence, the p-polarized spectra are blue-shifted.

For the 1st and subsequent SBs, the impact of an angle of incidence of $\varphi = 15°$ on the spectrum is not large, while for $\varphi = 30°$ it is considerable. As the order of the SBs increases, the impact of changing the angle of incidence to $\varphi = 30°$ is greater, leading to a significant shift of SBs from their original position, taken at $\varphi = 0°$.

An FTS 6000 FTIR spectrometer, in conjunction with a UMA-500 IR microscope, was used for the experimental investigations of 1D PCs. The microscope objective (see Fig. 2) contains two lenses, M1 and M2. If the objective is operated in reflection mode, the incident light falls on half of lens M1 and reflects off it, forming a divergent beam. This divergent beam returns by reflection off the other halves of lenses M2 and M1 before reaching the detector. Because of the construction of the objective, the light beam converging on the object is in the shape of a truncated half-cone (Fig. 2(b)). This shape is due to the fact that light with an angle of incidence close to the normal is not collected.
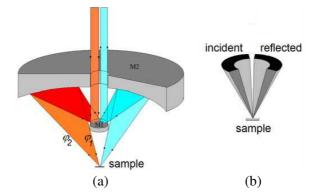

Figure 2. (a) Schematic of the beam path in IR microscope, showing mirrors M1 and M2 during measurements of reflection spectra R; (b) Shape of incident and reflected light, as truncated semi-cone volumes.

From Fig. 2(b), we use a converging beam model, comprising a set of beams with angles of incidence φ. Let us restrict this set of angles using two parameters: the minimal and maximal angles of incidence, φ_1 and φ_2, respectively (Fig. 2(a)). The range of angles between them, $\Delta\varphi = \varphi_1 \div \varphi_2$, is the parameter describing the convergence. We divide the range of converging $\Delta\varphi$ into specific angles of incidence, φ, with a step size of $\delta\varphi = 1°$. For each of these angles, we calculate the reflection spectra $R_\varphi(\lambda)$. Finally, we average the spectra obtained, assuming that all of the angles of incidence contribute equally to the

average spectrum $R_{\Delta\varphi}(\lambda)$, according to the following expression (1)

$$R_{\Delta\varphi}(\lambda) = \frac{1}{k}\sum_{\varphi2}^{\varphi1} R_{\varphi}(\lambda)$$ (1)

where the number of selected angles, $k = \Delta\varphi/\delta\varphi$. Let us introduce two types of focused light beams: one with $\varphi_1 = 5°$ and $\varphi_2 = 20°$, and the second with $\varphi_1 = 10°$ and $\varphi_2 = 30°$. In the first case, the number of distinct angles, k, for averaging the spectra $R_{\varphi}(\lambda)$ is 16, while in the second case it is 21. Note that in the second case, the convergent beam is more intense. As mentioned earlier, because of the geometry of the setup, in both cases angles close to normal are absent. A schematic diagram of the light cones incident on the PC for the two selected ranges of angles $\Delta\varphi = 5$–$20°$ and $\Delta\varphi = 10$–$30°$ is shown in Figs. 3(a) and 3(b). In Fig. 3(c), reflection spectra calculated for normal incidence, as well as for $\Delta\varphi = 5$–$20°$ and $\Delta\varphi = 10$–$30°$, are shown.
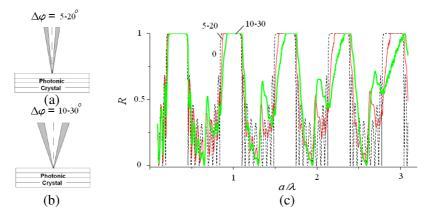

Figure 3. Model of focused beam in the range $\Delta\varphi = $ (a) $5 \div 20°$, (b) $10 \div 30°$; (c) p-polarized average spectrum $R_{\Delta\varphi}(\lambda)$ calculated using models in Figs. 3(a) and 3(b). The numbers beside the spectra correspond to the range of angles $\Delta\varphi$ in degrees.

From Fig. 3(c), bands with High Reflection (HR), with the exception of the first HR band, are deformed compared to those obtained using normal incidence of light. For $\Delta\varphi = 10$–$30°$, the shape of the HR bands, starting with the 3rd band, are deformed from a Π-type shape with a flat maximum to one with an irregular maximum. This is expected, since an increase in the angle of incidence φ leads to a narrowing of the HR bands, mainly due to the significant blue shift of the red edge of the SB at oblique incidence of light. Moreover, in an

averaged spectrum $R_{\Delta\varphi}(\lambda)$ (Fig. 3(c)) a smoothing of the interference oscillations between the HR bands is apparent, due to the summation of these narrow interference bands for different incident angles. This smoothing effect increases with an increase in the HR's order.

Clearly, convergence in the probe beam deforms and shifts the HRs, and the effect increases with an increase of the HR's order. The next step was to explore these effects using a gap map presentation [1]. A map of the stop-bands can be calculated over a wide range of the filling fractions, f, from 0 to 1 [16]. It is worth noting that, in this system, practically the entire range of filling fractions can be achieved technologically. The advantages of the gap map approach have been demonstrated in our previous studies, looking at the design of a variety of one-dimensional (1D) PCs, including disordered [17], composite [18], omnidirectional [19], three-component [20] and resonator [21] structures.

3. INVESTIGATION OF INFLUENCE OF LIGHT BEAM CONVERGENCE USING A GAP MAP APPROACH

In our calculations of the PBGs gap map, we used over 100 values of the parameter f_{Si} in the range 0.01 to 0.99. From the calculated R spectra, values of a/λ satisfying the condition $R_{cutoff} > 0.99$ are selected and plotted on a graph with coordinates of f_{Si} versus a/λ. The PBG map obtained is presented in Fig. 4, from which the main (or 1st) SB and a number of SBs of high order, labeled 1 to 49, and others, are observed for p-polarized light (see Fig. 1). The numbers of SBs on the map are variable, because some SB areas may not show up in the spectrum, depending on the filling fraction. Therefore, the number of SBs on the map is different from the number of high reflection bands in the spectrum R. The areas of p-polarised SBs for two converging beams with parameters $\Delta\varphi = 5 \div 20°$ and $\Delta\varphi = 10 \div 30°$ are also shown in Fig. 4.

Figure 4 shows how the areas of SBs for the focused beam change on the map with an increase in the SB order. As the order of SBs increase, a shift in the the red edge of the SBs is observed for all filling fractions. As explained earlier, this is related to the influence of high angle incident beams on the calculation of the average $R_{\Delta\varphi}(\lambda)$ spectrum.

Therefore, by analyzing the SB map, we can predict the influence of light beam convergence on the SBs and, consequently, on the HR bands in the reflection spectrum. In some cases this influence is insignificant, while in others it may cause the deformation of SBs when compared with an unfocused beam at normal incidence of light.
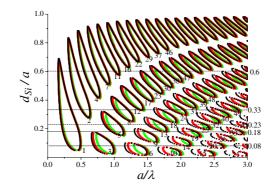
Figure 4. Maps of the photonic band-gap areas of a 1D PC comprising a periodic Si-Air structure with $m = 4$, calculated for normal incidence of light ($\Delta\varphi = 0$, black line) and for p-polarized beams with focusing parameters of $\Delta\varphi = 5 \div 20°$ (red line) and $\Delta\varphi = 10 \div 30°$ (green line). The horizontal dashed lines crosses the SB areas of PCs with specific filling fractions, for example $f_{Si} = 0.23$ for $\lambda/4$-layers.

4. EXPERIMENTAL EVALUATION OF THE INFLUEN-CE OF THE CONVERGENCE OF THE LIGHT BEAM ON THE SBS

For this study, 1D PC structures were fabricated using optical lithography and anisotropic etching. Anisotropic chemical etching was used for microstructuring of the (110) Si [13], because this technology generates high quality, mirror-like, Si side-walls, resulting in excellent infrared spectra. Thermally grown silicon dioxide was used as a mask when etching the wafers. The etching depth, and therefore, the wall height of the Si-air periodic structures (Fig. 5) varied from 20 to 50 μm.

The etch depth is dictated by the size of the IR microscope aperture used in the characterization setup. In our case, the microscope was combined with an FTIR FTS 6000 spectrometer in reflection, R, mode in the wavenumber range $\nu = 650$–$6500\,\text{cm}^{-1}$ (wavelength $\lambda = 1.5$–$15\,\mu\text{m}$) [13]. A gold coated glass slide was used as a 100% reflection reference. For polarized infrared measurements, with the focused light beam incident normal to the sample surface, the electric vector of the incident light is aligned with the Si grooves for E-polarized light, while for H-polarized light the electric vector is aligned along the depth direction of the grooves, as shown in Fig. 5. Therefore, the E-polarized light corresponds to s-polarization while the H-polarized light to p-polarization. The experimental spectra R have been normalized and are scaled in arbitrary units (a.u.) due to the influence of the shading
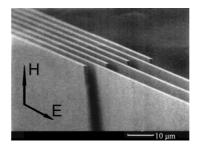
Figure 5. SEM image of a 1D PC with an inter-digital design. The number of periods, $m = 6$, and the images shows the directions of the electric field vectors, for E- and H-polarization, of the incident light.

effect of the Si substrate [13].

According to Ref. [14], n_{Si} in the mid-infrared spectral range is ~ 3.421, while in the near-IR range it increases to $n_{Si} \sim 3.45$ (Fig. 6(a)). Since both spectral ranges are covered in our experiments, it was necessary to identify the effect of n_{Si} dispersion on SB shift during our calculations. So, we performed the calculation using a constant value of $n_{Si} = 3.421$, as well as doing the same calculation taking into account the dispersion of $n_{Si}(\nu)$. Reflection spectra for the
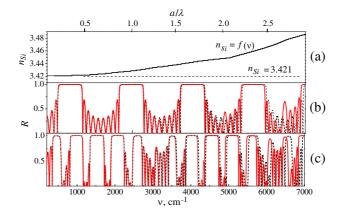

Figure 6. (a) Dispersion of the refractive index $n_{Si}(\nu)$ from Ref. [14] and the reflection spectra, R calculated with (red thin line) and without (black dotted line) dispersion of n_{Si} for a 1D PC based on a Si-Air structure. The lattice constant, $a = 4\,\mu m$, and the number of periods, $m = 6$. The filling fraction, (b) $f_{Si} = 0.23$ and (c) 0.6 at normal incidence of light.

PC were calculated for two values of filling fraction, $f_{Si} = 0.23$ and $f_{Si} = 0.6$, at normal incidence of light and are presented in Figs. 6(b) and 6(c), respectively. It is evident from these figures that a significant shift of the SB edges for both filling fractions begins to appear for $\nu > 5000\,\text{cm}^{-1}$ ($\lambda < 2\,\mu\text{m}$). Thus, given that our measurements cover the near-IR spectral range, where all the high order SBs are located, all subsequent calculations for fitting the experimental spectra were performed taking into account refractive index dispersion.

For experimental verification of the theoretical results, two samples with different f_{Si} values, namely 0.6 and 0.18, were selected. The first 1D "Si-air" photonic crystal selected had 6 periods, a lattice constant of $a = 4\,\mu\text{m}$ and a sufficiently large filling fraction, $f_{Si} = 0.6$, to minimize any possible impact of thickness inhomogeneities in the Si walls [17]. Fig. 7(a) presents measurements of E-and H-polarized R spectra for this sample, exhibiting a large number of pronounced bands of high reflection across the entire spectral range from 650 to
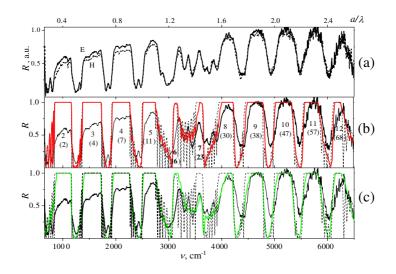

Figure 7. (a) Polarized experimental reflection, E-, and, H-, spectra of a 1D PC, based on a Si-Air structure. The lattice constant, $a = 4\,\mu\text{m}$, the number of periods, $m = 6$, the filling fraction, $f_{Si} = 0.6$ and the refractive index of the incoming and outgoing media, $n = 1$; (b), (c) Calculated spectrum (dashed line) for normal incidence of light (unfocused beam), fitted to the experimental E-spectrum (thick black line taken from the graph (a)), and p-spectra calculated using a model of a focused beam for (b) $\Delta\varphi = 5 \div 20°$ (thin red line) and (c) $\Delta\varphi = 10 \div 30°$ (thin green line).

$6500\,\mathrm{cm}^{-1}$. The E- and H-spectra are almost identical, indicating the absence of anisotropy in the properties of the periodic structure, as expected in 1D PCs of this type. This effect is general, that is, it was observed in all our measurements. So, subsequent comparisons with the calculated spectra were carried out for the E-polarized experimental spectra only.

Figure 7(b) shows the calculated spectrum R for the unfocused beam, the dashed line, fitted to the experimental spectrum, the thick black line. Fitting parameters of $d_{Si} = 2.38\,\mu\mathrm{m}$ and $d_{air} = 1.62\,\mu\mathrm{m}$ were used. Given that the lattice constant $a = 4\,\mu\mathrm{m}$, the PC parameters obtained correspond to a value for the filling fraction of $f_{Si} = 0.6$. The positions of the HR bands in the calculated and experimental spectra are generally in good agreement, as are the gaps between them. This suggests that there are no significant thickness inhomogeneities in the fabricated structure. In the experimental spectra, shown in Fig. 7(a), the tendency of the shape of the HR bands to deform, from a Π-type to bands having an approximately triangular shape, as the wavenumber, ν, increases is clear. A similar trend was noted in the data presented in Fig. 3, when beam convergence was introduced, suggesting that beam convergence is the source of this deformation.

Reflection spectra calculated taking into account beam focusing for $\Delta\varphi = 5 \div 20°$ for p- and s-polarizations are identical, therefore, in Fig. 7(b), only one p-spectrum is shown. The experimental E-spectrum is also shown on the same graph. Spectra calculated for focused and unfocused light beams are practically coincident over the entire spectral range, with the exception of $\nu = 3000$–$3800\,\mathrm{cm}^{-1}$. Two numbers are shown for each HR band in Fig. 7(b). The top number is the sequence number of the SBs in the spectrum, while the number in brackets is the number of the SBs on the map. Two bands (HR-6 and HR-7) are seen in the spectral range $\nu = 3000$–$3800\,\mathrm{cm}^{-1}$ in which the position of the red edge of the bands is very different. It is clear that the experimental spectral bands, HR-6 and HR-7, are strongly suppressed in comparison with the calculated HRs for the unfocused beam.

If we transform the values of ν on the x-axis to units of a/λ, as shown in the upper x-axis scale in Fig. 7, we can compare it to the SBs shown in Fig. 4. Let us explore how the line for the value of the filling fraction $f_{Si} = 0.6$ crosses the SBs, in order to reveal the corresponding HR bands in the reflection spectrum. The absence of the first SB is because it is, from Fig. 4, in the range 0.2–0.25 of a/λ, which corresponds to a spectral range of λ from 20 to 23 $\mu\mathrm{m}$ (or ν range from 500 to $430\,\mathrm{cm}^{-1}$). Therefore, this band is outside the spectral range measured by our spectrometer (650–$6500\,\mathrm{mm}^{-1}$).

A calculated p-spectrum, with beam focusing in the range $\Delta\varphi = 10 \div 30°$, is shown in Fig. 7(c). First, the calculated band HR-7 is suppressed, as in the experiment. Secondly, in the p-spectrum, the HR-8 band demonstrates a more dramatic shift of the red edge, compared to the p-spectrum for $\Delta\varphi = 5 \div 20°$, and even more so with the spectrum for $\Delta\varphi = 0$. Also, the calculated HR-8 band is similar in shape to the experimental band HR-8.

In order to clarify this behaviour, let us select and magnify a portion of the map of Fig. 4 and superimpose it on fragments of the spectra from Figs. 7(b) and 7(c) in the spectral range corresponding to the bands HR-5÷HR-9 in the R spectrum. By doing this, we obtain Fig. 8. Fig. 8 shows that there are no other SB areas on the map between SBs 16 and 17, but on the calculated spectrum the additional HR band is visible, although it is quite narrow. We have designated
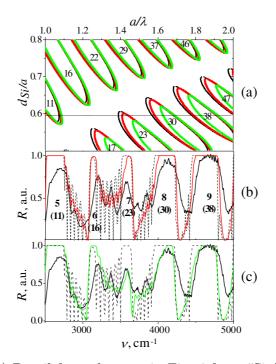

Figure 8. (a) Detail from the map in Fig. 4 for a "Si-Air" PC. The number of periods, $m = 6$, $a = 4\,\mu$m and the filling fraction, $f_{Si} = 0.6$; (b), (c) Detail from the experimental E-spectrum from Fig. 7(b) (thick black line) and the spectrum calculated for an unfocused beam for $\Delta\varphi = 0$ (dashed black line). Spectra calculated with an unfocused beam model are shown for (b) $\Delta\varphi = 5 \div 20°$ by the thin red line and for (c) $\Delta\varphi = 10 \div 30°$ by the thin green line.

this band HR-6. This can be explained by the fact that, if the PC considered is a multiperiod structure (with $m \geq 10$), then the PBG will be extended and approach stop bands 16 and 17 (and other SBs). In the ideal case, for an infinite PC, this effect will cause a joining of edges of all SB areas. In this case, the HR-6 band reaches 100% reflection in the spectrum and will expand on the map. So, we can assume that this band is the SB, suppressed due to the small number of periods ($m = 6$) used during calculations, and, therefore, identify it with the number 16. The band HR-7 in the spectrum for normal incidence is well formed and, therefore, appears on the SB map (SB-23). When using a focused beam with $\Delta\varphi = 5 \div 20°$ the position of the red edge of the HR-7 is blue shifted relative to this region for $\Delta\varphi = 0$, but some parts of this band have R close to 100%, and so it is easily observed. But in the experimental spectrum this band is suppressed.

Increasing the focusing of the light beam to $\Delta\varphi = 10 \div 30°$, causes strong deformation of the band HR-7, to the extent that is almost totally suppressed. Bands HR-8 and HR-9 are deformed to a lesser extent, but do exhibit a large shift in the red edge of the HRs (Fig. 8(c)).

In the experimental spectrum, shown in Figs. 8(b) and 8(c), smoothing of the interference fringes between the bands HR-5 and HR-8 is observed compared with the calculated spectra for normal incidence of light. This behavior is also observed with other SBs, supporting the use of a focused beam model. Using this approach, we obtained good agreement in the shape of bands HR-8 and HR-9 with experiment. We also noted the suppression of band HR-7, which allows to make a reasonable conclusion on the influence of beam focusing on SBs. The model used the beam parameter $\Delta\varphi = 10 \div 30°$ for beam convergence, considered most likely by comparison with experimental data. It should be noted that the increase in focusing parameter, for example to $\Delta\varphi = 15 \div 35°$, causes a significant shift in the HR bands, as well as band deformation. This adversely impacts the agreement of the experimental HR bands position with the bands in the fitted spectra obtained using this model.

In general, the impact of beam focus for a specific PC with $f_{Si} = 0.6$ has no effect on the position of the SBs, when compared with calculations for normal incidence, with the exception of the few SBs mentioned earlier. These SBs are more sensitive to the focused beam, due to their location at the SB edges on the gap map.

To confirm the trends identified above, a second sample with a lower $f_{Si} = 0.18$ and a lattice parameter of $a = 3\,\mu m$ was investigated. A section of the SB map for this PC is shown in Fig. 9(a), and experimental and the calculated spectra for normal incidence of light
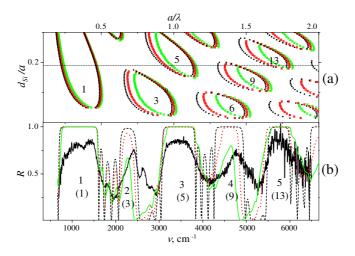
Figure 9. (a) Gap-map for 1D PC (Si-Air, $a = 3\,\mu\text{m}$, $m = 4$), calculated for normal incidence of light beam (black dotted line) and for p-polarized beams with beam focusing parameters $\Delta\varphi = 5 \div 20°$ (red dotted line) and $\Delta\varphi = 10 \div 30°$ (green dotted line); (b) Calculated R spectra, fitted to the experimental spectrum (shown by the thick black line) at $f_{Si} = 0.18$ for normal incidence of the light beam (black dashed line) and using a model incorporating beam focusing with parameters $\Delta\varphi = 5 \div 20°$ (thin red line) and $\Delta\varphi = 10 \div 30°$ (thick green line).

and focused beams with two parameters of $\Delta\varphi$ are shown in Fig. 9(b). Calculated spectra, obtained as a result of a fit to the experimental data, show good agreement with the first band HR-1 to SB-1, as well as to those of HR-3, HR-4, HR-5, to Stop-Bands SB-5, SB-9 and SB-13 on the map (Fig. 9(a)). Spectra calculated taking into account beam focusing exhibited significant edge deformation for the HR-2 (SB-3) and HR-4 (SB-9) bands, compared to those calculated for normal angles of incidence. This is because Stop Bands SB-3 and SB-9 are situated on the map where their properties are extremely sensitive to beam focusing. For calculated spectra, these HR bands deform significantly as a result of the introduction of beam convergence. Their shape is similar to those of the experimental bands, in particular, to the bands of HR-2 and HR-4, for a focus parameter, $\Delta\varphi = 10 \div 30°$. The location of SB-1 and SB-5 on the map is such, that the effect of beam focus on the deformation of their edges is not significant.

In summary, the effect of beam focusing on SB characteristics has been experimentally investigated using reflection spectra from PCs for two different filling factors. Good agreement is achieved for a focused beam parameter, $\Delta\varphi = 10 \div 30°$.

5. CONCLUSION

In this paper, we have demonstrated that for one-dimensional photonic crystals the impact of the beam convergence with values of $\Delta\varphi$ between $10°$ and $30°$ has no effect on the position of the SBs for the first and nearest SBs, compared with calculations performed for normal beam incidence, with the exception of a small number of SBs which are more sensitive to the focused beam due to their location at the edges of SBs on the map. For higher-order SBs and for PCs with low-value fractions of the high refractive index component, the effect of the beam convergence can be significant. Good agreement was obtained between experimental reflection spectra from one-dimensional photonic crystals with a variety of filling fractions, and calculations made using a model incorporating a focused beam.

It is also shown that one-dimensional photonic crystals are an effective model for the study of the influence of beam focus on the stop-bands of photonic structures, as they have many secondary photonic bands, which are more sensitive to beam focus. Optical characterization of photonic structures is generally performed using a focused beam. This study of the impact of the effect of focus should enable an improvement of the optical quality of PCs obtained by microstructuring of silicon. The results are applicable across a wide wavelength range, from the visible to far-infrared, and assist in the engineering of Si based photonic elements for use in optical communication, integrated-optics and display technologies [22–26].

ACKNOWLEDGMENT

REFERENCES

1. Joannopoulos, J. D., S. G. Johnson, J. N. Winn, and R. D. Meade, *Photonic Crystals. Molding the Flow of Light*, 2nd Edition, Princeton University Press, Princeton, 2008.

2. Lourtioz, J.-M., H. Benisty, V. Bergerm, J.-M. Gerard, D. Maystre, and A. Tchelnokov, *Photonic Crystals: Towards Nanoscale Photonic Devices*, Springer-Verlag Berlin Heidelberg, 2005.

3. Soref, R., "The past, present and future of silicon photonics," *IEEE J. Select. Top. Quantum Electr.*, Vol. 12, 1678–1687, 2006.

4. Almeida, V. R., C. A. Barrios, R. R. Panepucci, and M. Lipson, "All-optical control of light on a silicon chip," *Nature*, Vol. 431, 1081–1084, 2004.

5. *Topics in Applied Physics 119: Silicon Photonics II Components and Integration*, D. J. Lockwood and L. Pavesi, Eds., Springer-Verlag Berlin Heidelberg, 2011.

6. Baldycheva, A., V. Tolmachev, T. Perova, Y. Zharova, E. Astrova, and K. Berwick, "Silicon photonic crystal filter with ultrawide passband characteristics," *Optics Letters*, Vol. 36, No. 10, 1854–1856, 2011.

7. Barillaro, G., S. Merlo, S. Surdo, L. M. Strambini, and F. Carpignano, "Integrated optofluidic microsystem based on vertical high-order one-dimensional silicon photonic crystals," *Microfluid Nanofluid*, Vol. 12, 545–552, 2012.

8. Ghulinyan, M., C. J. Oton, G. Bonetti, Z. Gaburro, and L. Pavesi, "Free-standing porous silicon single and multiple optical cavities," *J. Appl. Phys.*, Vol. 93, No. 12, 9724–9729, 2003.

9. Gruning, U., V. Lehmann, S. Ottow, and K. Busch, "Macroporous silicon with a complete two-dimensional photonic band gap centred at 5 μm," *Appl. Phys. Lett.*, Vol. 68, 747–749, 1996.

10. Krauss, T. F. and R. M. de La Rue, "Optical characterization of waveguide based photonic microstructures," *Appl. Phys. Lett.*, Vol. 75, 3063–3065, 1999.

11. Rowson S., A. Chelnokov, C. Cuisin, and J.-M. Lourtioz, "Two-dimensional photonic bandgap reflectors for free-propagating beams in the mid-infrared," *J. Opt. A: Pure Appl. Opt.*, Vol. 1, 483–489, 1999.

12. Nguyen, H. C., P. Domachuk, B. J. Eggleton, M. J. Steel, M. Straub, M. Gu, and M. Sumetsky, "New slant on photonic crystal fibers," *Opt. Exp.*, Vol. 12, No. 8, 1528–1539, 2004.

13. Tolmachev, V. A., T. S. Perova, E. V. Astrova, B. Z. Volchek, and J. K. Vij, "Vertically etched silicon as 1D photonic crystal," *Phys. Stat. Solidi (a)*, Vol. 197, No. 2, 544–549, 2003.

14. Palik, E. D., Ed., *Handbook of Optical Constants of Solids*, Academic Press, Inc., NY, 1985.

15. Azzam, R. M. A. and N. M. Bashara, *Ellipsometry and Polarized Light*, North-Holland, Amsterdam, Netherlands, 1977.

16. Tolmachev, V., T. Perova, E. Krutkova, and E. Khokhlova, "Elaboration of the gap map method for the design and analysis of one-dimensional photonic crystal structures," *Physica E: Low-dimensional Systems and Nanostructures*, Vol. 41, 1122–1126,

2009.

17. Tolmachev, V. A., A. V. Baldycheva, K. Berwick, and T. S. Perova, "Influence of fluctuations of the geometrical parameters on the photonic band gaps in one-dimensional photonic crystals," *Progress In Electromagnetic Research*, Vol. 126, 285–302, 2012.

18. Tolmachev, V. A., T. S. Perova, S. A. Grudinkin, V. A. Melnikov, E. V. Astrova, and Y. A. Zharova, "Electro-tunable in-plane one-dimensional photonic structure based on silicon and liquid crystal," *Appl. Phys. Lett.*, Vol. 90, No. 1, 011908/1–3, 2007.

19. Tolmachev, V. A., T. S. Perova, J. Ruttle, and E. V. Khokhlova, "Design of one-dimensional photonic crystals using combination of band diagram and photonic gap map approaches," *J. Appl. Phys.*, Vol. 104, No. 3, 033536, 2008.

20. Tolmachev, V. A., A. V. Baldycheva, S. A. Dyakov, K. Berwick, and T. S. Perova, "Optical contrast tuning in three-component one-dimensional photonic crystals," *J. of Lightwave Tech.*, Vol. 28, No. 10, 1521–1529, 2010.

21. Tolmachev, V. A., V. A. Melnikov, A. V. Baldycheva, K. Berwick, and T. S. Perova, "Electrically tunable Fabry-Perot resonator based on microstructured Si containing liquid crystal," *Progress In Electromagnetic Research*, Vol. 122, 293–309, 2012.

22. Liu, C.-C. and C.-J. Wu, "Near infrared filtering properties in photonic crystal containing extrinsic and dispersive semiconductor defect," *Progress In Electromagnetic Research*, Vol. 137, 359–370, 2013.

23. Hung, H.-C., C.-J. Wu, T.-J. Yang, and S.-J. Chang, "Enhancement of near-infrared photonic band gap in a doped semiconductor photonic crystal," *Progress In Electromagnetics Research*, Vol. 125, 219–235, 2012.

24. Wu, C.-J., T.-J. Yang, C.-C. Li, and P.-Y. Wu. "Investigation of effective plasma frequencies in one-dimensional plasma photonic crystals," *Progress In Electromagnetics Research*, Vol. 126, 521–538, 2012.

25. Chang, T.-W., J.-J. Wu, and C.-J. Wu, "Complex photonic band structures in a photonic crystal containing lossy semiconductor InSb," *Progress In Electromagnetics Research*, Vol. 131, 153–167, 2012.

26. Yong, Z. H., Z. F. Chen, Y. H. Chen, C. W. Leung, H. Lai Wa Chan, B. Li, and Y. Wang, "Temporal modulation of light intensity via 1D time-variant photonic crystal structure," *Progress In Electromagnetics Research*, Vol. 135, 627–639, 2013.